Lawrence Berkeley Laboratory
UNIVERSITY OF CALIFORNIA

ENERGY & ENVIRONMENT
DIVISION

Presented at the General Motors Research Laboratory Conference,
Particulate Carbon: Atmospheric Life Cycle, Warren, MI,
October 12-14, 1980

GRAPHITIC CARBON IN URBAN ENVIRONMENTS AND THE ARCTIC

H. Rosen, A.D.A. Hansen, R.L. Dod, L.A. Gundel, and
T. Novakov

October 1980

Prepared for the U.S. Department of Energy under Contract W-7405-ENG-48

DISCLAIMER

GRAPHITIC CARBON IN URBAN ENVIRONMENTS AND THE ARCTIC*

H. Rosen, A.D.A. Hansen, R.L. Dod, L.A. Gundel, and T. Novakov
Lawrence Berkeley Laboratory
University of California
Berkeley, California 94720

Introduction

Recent measurements of aerosol particles indicate the presence of a large optically absorbing component which can cause visibility degradation and climatic effects. The nature of this absorbing species has been investigated by a variety of modern methods of analysis, which has led to its identification on a microscopic level as graphitic (black) carbon [1]. In our paper this methodology will be described and extended to the quantification of graphitic carbon and its absorption coefficient. New results from the Arctic will also be presented, which show the presence of graphitic carbon concentrations comparable to those found in urban environments. In Section I of this paper, the LBL laser transmission method will be described and compared to photoacoustic measurements [2] and measurements using the integrating plate method [3]. A theoretical model will be presented which gives physical insight into why these transmission methods selectively measure the absorbing properties of the aerosol and are insensitive to its scattering properties. In Section II the use of Raman spectroscopy to identify the optically absorbing species in urban particulates will be described. In Section III preliminary results using a thermal analysis technique [4] for quantifying the graphitic carbon content of the aerosol will be presented. Finally, in Section IV the methods of analysis described above will be applied to the characterization of the carbonaceous aerosol in the Arctic.

I. Determination of the Absorption Coefficient of Aerosol Particles by the Laser Transmission Method

The LBL laser transmission method is an extension of the integrating plate

*This work was supported by the Biomedical and Environmental Research Division of the U.S. Department of Energy under contract No. W-7405-ENG-48 and by the National Science Foundation.

technique [5] to certain other filter media (Millipore, quartz fiber, Teflon), which act as an efficient collection substrate as well as play the role of the opal glass as a diffuse scatterer. The laser transmission apparatus compares the transmission of a 633-nm He-Ne laser beam through a loaded filter relative to that of a blank filter (Fig. 1). The loaded filters are placed in the beam with the loaded side towards the laser; after multiple scattering through the filter substrate, the light is collected by an f/1 lens and focused on a photomultiplier tube. The absorption coefficient, σ_{ab}, is determined from the Beer-Lambert Law in a fashion similar to that outlined for the integrating plate method. This method measures the absorbing component of aerosol particles and is apparently insensitive to its scattering properties, as was demonstrated by a photoacoustic study [2].

Unlike conventional optical absorption techniques, photoacoustic spectroscopy measures the energy deposited in a sample due to absorption. Since questions have been raised whether the LBL laser transmission method exclusively measures the absorbing rather than the scattering component of the aerosol, a comparison between photoacoustic and optical attenuation measurements made on the same aerosol sample should help resolve this ambiguity.

The photoacoustic measurements were made in an acoustically nonresonant detector with cylindrical geometry (Fig. 2). A Knowles microphone (Model BT-1759) was used, and the cell dimensions were 2.1 cm in diameter and 0.3 cm in length. The gas in the detector cell was air at atmospheric pressure. An He-Ne laser operating at 632.8 nm with 0.5 mW of power was used as the light source, and the experiments were performed at a modulation frequency of 20 Hz. The aerosol particles, collected on 1.2-μm Millipore filter substrates, were mounted on a 1.5-mm-thick Pyrex backing with the particles facing the incident light beam. Experiments were also performed with the laser beam first incident on the filter substrate.

It is easy to show in the limit of low frequency light modulation [6] ($\leq$ 100 Hz) that the ratio of the photoacoustic signal to a reference sample for which the signal is saturated is given by:

$$S_{ph} = V/V_{sat} = 1 - \exp(-\alpha\ell) \ .$$

This saturable behavior was observed for highly absorbing samples, and the sample which yielded the largest photoacoustic signal was used as the reference, V_{sat}. Note that such samples yield values of $\alpha\ell \geq 3$, as deduced from the optical attenuation measurements; hence the highest signal obtained from available samples is close to the actual saturation value.

The experimental setup for the optical attenuation measurements is described above. In this technique the signal S_{op} is defined as $1 - \exp(-x)$, where x is the optical attenuation of the sample and is given by $-\ln I/I_0$, where I is the transmitted intensity of a loaded filter and I_0 is the transmitted intensity of a blank filter.

In Fig. 3 we present a plot of the normalized photoacoustic signal S_{ph} vs. S_{op} for a wide range of ambient samples and samples collected directly from combustion sources. The samples include urban particulates collected over a 24-hr period in Fremont and Anaheim, California; Denver, Colorado; and New York, New York; and particles collected in a highway tunnel and from an acetylene torch. The least squares fit of the experimental points yields a correlation coefficient r of 0.98 and a slope of 1.03, which would be expected if both techniques measure the same optical property of the aerosol particles. Since the photoacoustic signal is proportional to the heat generated by absorption, we conclude that the optical-attenuation method measures the light-absorbing component of the aerosol particles.

From a theoretical point of view, this result is somewhat surprising,

since aerosol particles have a large scattering coefficient, which would be expected to contribute to the optical attenuation measurement and not to the photoacoustic signal. This is especially true where the absorbing component represents only a small fraction of the aerosol mass. In this paper a simple model calculation will be presented which explains these observations and points out the critical role of the filter substrate as an almost perfect diffuse reflector in the technique. Similar considerations may also apply to the opal glass method used by Weiss et al. [7].

For this model calculation, we will assume that the particles and the filter media can be treated independently and consider the geometry shown in Fig. 4. A similar treatment, where the light beam is first incident on the particles, gives identical results. After the light beam passes through the filter medium, it is incident on the particles with an intensity, I_0. The particles forward scatter a fraction of the incident light, backward scatter a fraction, and absorb a fraction. These components in the low loading limit are respectively given by $n_s\sigma_F I_0$, $n_s\sigma_B I_0$, and $n_A\sigma_A I_0$, where n_s is the number of scattering aerosol particles per unit area, n_A is the number of absorbing aerosols per unit area, σ_F is the forward scattering cross section, σ_B is the backward scattering cross section, and σ_A is the absorption cross section.

Since the optical attenuation technique only measures the forward scattering light, it would seem as if the backscattered light would be lost to the system and would contribute to the attenuation. However, the filter, in our method, is almost a perfect reflector. Under these circumstances, the backscattered light will be reflected in the forward direction and will again be incident on the particles. This process will continue until almost all the backscattered radiation is collected by the optics and therefore does not contribute to the optical attenuation. This result can be put in mathematical form, where I is

the light detected by the collection optics and R_F is the reflectivity of the substrate.

$$I = I_0(1 - n_s\sigma_b - n_A\sigma_A) + I_0(1 - n_s\sigma_B - n_A\sigma_A)n_s\sigma_B R_F \quad (1)$$
$$+ I_0(1 - n_s\sigma_B - n_A\sigma_A)n_s^2\sigma_B^2 R_F^2 + \ldots I_0(1 - n_s\sigma_B - n_A\sigma_A)n_s^n\sigma_B^n R_F^n$$
$$= I_0 \frac{(1 - n_s\sigma_B - n_A\sigma_A)}{(1 - n_s\sigma_B R_F)} .$$

Consider several limits. Where $R_F \simeq 0$, which normally would be considered an ideal substrate, Eq. (1) reduces to

$$I = I_0(1-n_s\sigma_B - n_A\sigma_A) .$$

Under these conditions the backscattered radiation will contribute significantly to the optical attenuation and make the technique unsuitable for exclusively measuring the absorbing properties of the aerosol. In our method, however, $R_F \simeq 1$ and Eq. (1) becomes

$$I = I_0(1 - \frac{n_A\sigma_A}{1 - n_s\sigma_B}) .$$

Or the optical attenuation in the low loading limit is

$$ATN = I_0 - I = \frac{I_0 n_A\sigma_A}{1-n_s\sigma_B} .$$

From this expression it is clear that a nonabsorbing aerosol will make no contribution to the optical attenuation; this is consistent with our experimental results. The magnitude of the optical attenuation is somewhat dependent on the scattering properties of the aerosol; however, in the low loading limit, this effect is small. For example, if the substrate has 50% coverage, and if the scattering cross section of the particles, σ_s, is twice the particle area,

then $n_s\sigma_s \simeq 1$. If σ_B is about 20% of σ_s (the maximum value measured by Charlson and his coworkers [8]), then

$$1 - n_s\sigma_B \simeq .8 \ ;$$

so that even for this rather high loading, the error in the absorption measurement due to scattering of the aerosol is only about 20%. This treatment should only be viewed as giving physical insight into the LBL method for determining absorption coefficients and clearly is approximate since it assumes that the scattering properties of the particles are not affected by the filter substrate and neglects the penetration of the particles into the substrate. Future analysis will try to evaluate the significance of these effects.

The LBL laser transmission method has been compared to the integrating plate technique [5] developed at the University of Washington. Five sampling sites in the western part of Washington state were used in this study, from a highly congested site in a highway tunnel to a very remote site on a western foothill in the Olympic Mountains. By sampling such diverse aerosol conditions, the range of absorption coefficients of the air samples was more than three orders of magnitude, from $\sim 10^{-7}$ m^{-1} to nearly 10^{-3} m^{-1}, with the total carbon concentration ranging from about 5 $\mu g/m^3$ (Mt. Octopus) to nearly 90 $\mu g/m^3$ (highway tunnel).

The result of these comparisons [3] are shown graphically in Fig. 5, where a plot of absorption coefficients is shown, as determined by the IPM using a Nuclepore substrate and the LTM using a Millipore substrate. A total of 44 filters of each type was used in this comparison. The correlation coefficient between the two measurements is 0.95, with the absorption coefficient determined by the LTM being greater than that determined by the IPM by a factor of approximately 2.5. The light absorption coefficients determined by these two methods are comparable and highly correlated. The reason for the higher

indicated absorption coefficient using the LTM could be due to several factors, including 1) penetration effects in the Millipore substrate, which could lead to enhanced absorption due to multiple scattering effects within the filter medium itself; 2) possible pile-up at the holes or loss of particles in the holes of the Nuclepore substrate; 3) differences in the collection efficiency of the two substrates. Studies are under way in both our laboratories to assess the magnitude of these effects. It should be emphasized, however, that the differences found between these two techniques are small in comparison with the large uncertainties reported in the literature for the magnitude of the absorbing component of aerosol particles. These differences are also small compared to the range of more than three orders of magnitude observed in the value of σ_{ab}.

II. Identification of Optically Absorbing Species in Urban Aerosols

Raman spectroscopy is a highly selective method of analysis, which, until recently, has not been applied to the characterization of air pollution particulates [9-11]. The technique can often be used to make unambiguous identifications since different chemical species have characteristic vibrational modes and therefore characteristic Raman spectra. The Raman spectroscopy apparatus uses a Coherent Radiation argon ion laser producing 1 W of power at 514 nm. The laser beam is focused by a 75-mm focal length cylindrical lens to a spot 0.06 mm x 2 mm on the sample surface via a small mirror, and the backscattered radiation is collected and imaged by an f/1 lens onto the slit of a 1-m Jarrell Ashe double monochromator equipped with 2 1180-grooves/mm gratings blazed at 5000 Å. The output of the spectrometer is detected by an FW130 photomultiplier cooled to -20°C and used in a photon-counting mode. The pulses, after appropriate shaping, are counted and displayed on a multichannel analyzer. A computer-controlled grating drive made by RKB, Inc., allows a given spectral

region to be scanned many times and added to the memory of the multichannel analyzer, greatly improving the SNR. In order to minimize heating effects, the highly absorbing samples used in these experiments are rotated at 1800 rpm by a motor, which increases the area illuminated by the laser beam by a large factor with almost no loss in signal level. The focal spot of the laser is located approximately 5 mm below the axis of rotation so that the effective illuminated area is an annulus of 5-mm radius and 2-mm width, resulting in the low power density of $\sim$ 1 W/cm^2.

The Raman spectra between 920 cm^{-1} and 1950 cm^{-1} of ambient, automobile exhaust, and diesel exhaust particulates are compared with the spectra of activated carbon and polycrystalline graphite in Fig. 6. It is evident that the spectra of activated carbon, diesel exhaust, automobile exhaust, and the ambient samples are very similar, with the positions of the two Raman modes coincident to within $\pm$ 10 cm^{-1} of the estimated experimental error. The ambient samples shown were collected as part of the RAPS program in St. Louis, Missouri and in the Arctic region near Barrow, Alaska. However, the same Raman modes are also evident in every urban sample studied so far (New York, Buffalo, Berkeley, Anaheim, Fremont). Koenig et al. [12] have studied the Raman spectrum of activated carbon and have identified the modes near 1600 cm^{-1} and 1350 cm^{-1} as being due to phonons propagating within graphitic planes. The close correspondence of the spectra in Fig. 6 indicates the presence of physical structures similar to activated carbon in both source and ambient samples. These graphitic species are formed directly in combustion, and throughout the text we shall use the term graphitic soot to describe them.

Urban and combustion source particulates collected on various filter media have a grey or black appearance. The graphitic species identified by Raman spectroscopy are the most likely candidate for explaining this coloration.

To test this hypothesis, we have developed an optical absorption technique to measure quantitatively various properties of the absorbing species (see above).

Using this apparatus we have studied the temperature stability and solubility of the absorbing species in ambient and source particulate samples. Our results show that these species have high temperature stability [13] with only minimal oxidation up to 400°C and are essentially insoluble in a wide variety of solvents [7,13]. We have also shown, using a spectrophotometer, that to within 20% over the visible spectral region, the optical attenuation has a $1/\lambda$ wavelength dependence characteristic of a constant imaginary index of refraction [7,13].

All these results strongly suggest that the absorbing species in urban and source particulate samples is graphitic soot. A direct substantiation of this hypothesis is provided by comparing the integrated intensity of the 1600-cm^{-1} Raman mode with the optical attenuation of the same filter sample. These measurements have been done on acetylene soot samples, which were essentially pure carbon with only trace amounts of metallic impurities; highway tunnel samples; and ambient samples collected in Berkeley and Fremont in the San Francisco air basin and Anaheim in the Los Angeles air basin. The results shown in Fig. 7 indicate that within experimental error there is a direct correspondence between the optical attenuation and the Raman intensity or graphitic soot content for all samples studied, despite widely different chemical compositions (e.g., for a given optical attenuation, the Pb and Fe concentrations vary by more than a factor of 100). The only reasonable explanation is that the optical attenuation is due to the graphitic soot content of the collected particulate.

In summary, we have shown that the species responsible for the high optical absorptivity of particulate samples has high temperature stability in air, is insoluble in a variety of solvents, and absorbs uniformly throughout the visible

We have also demonstrated that the amount of the absorbing species is directly proportional to the graphitic soot content as defined by Raman spectroscopy. All these results taken together indicate that the high optical absorptivity of both ambient samples collected in urban environments and various source particulate samples is due to the graphitic component of the aerosol.

III. Determination of Graphitic or Black Carbon Content of Aerosols by Combining Thermal Analyses with Optical Absorption Measurements

Malissa has reported a method of analysis [14] for the carbonaceous component of atmospheric aerosol particulate material by evolved gas analysis during a temperature-programmed combustion in oxygen. We have extended this analysis by constructing an apparatus which simultaneously measures the optical transmission of the particulate matter collected on a filter. Since the optical absorptivity of this material has been shown to be due to a graphitic component [1], this combination of analytical techniques may provide a direct determination of the light-absorbing fraction of the sample.

A schematic representation of the apparatus used in our analysis of carbonaceous material is shown in Fig. 8. The particulate sample, collected on a prefired quartz filter, is placed in the quartz combustion tube so that its surface is perpendicular to the tube axis. The tube is supplied with purified oxygen, excess oxygen escaping through an axial opening at the end of the tube. The remainder of the oxygen (together with gases produced during analysis) passes through a nondispersive infrared analyzer (MSA LIRA 202S) at a constant rate. Sample carbon may be evolved through volatilization pyrolysis, oxidation, or decomposition. To ensure complete conversion of this carbon to CO_2, a section of the quartz tube immediately outside the programmed furnace is filled with CuO catalyst, which is kept at a constant 900°C by a second furnace. This is especially necessary at relatively low temperatures when volatilization

and incomplete combustion are the dominant processes occurring.

The actual measurement consists of monitoring the CO_2 concentration as a function of the sample temperature. The result is a "thermogram," i.e., a plot of the CO_2 concentration vs. temperature, with the area under the thermogram proportional to the carbon content of the sample. The carbon content is quantitated by calibration with a calibration gas (CO_2 in oxygen) and by measuring the flow rate through the system. This calibration is crosschecked by analyzing samples of known carbon content.

The thermograms of ambient and source aerosol samples reveal distinct features in the form of peaks or groups of peaks. One important component of the carbonaceous aerosol is the graphitic carbon, which is known to cause the black or grey coloration of ambient and source particulate samples [1]. To determine which of the thermogram peaks corresponds to this graphitic carbon, we monitor the intensity of a He-Ne laser beam which passes through the filter. This provides simultaneous measurement of sample absorptivity and CO_2 evolution. The light penetrating the filter is collected by a quartz light guide and filtered by a narrow band interference filter to minimize the effect of the glow of the furnaces. An examination of the CO_2 and light intensity traces enables the assignment of the peak or peaks in the thermograms corresponding to the black carbon because they appear concurrently with the decrease in sample absorptivity.

The potential of this method (in the CO_2 mode) is illustrated in Figs. 9-11, where the complete thermograms of several source samples and an ambient sample are shown. The lower trace represents the CO_2 concentration, while the upper curve corresponds to the light intensity of the laser light beam that reaches the detector during the temperature scan. Inspection of the thermogram shows that a sudden change in the light intensity occurs concomitantly with

the evolution of a CO_2 peak. This demonstrates that the light-absorbing species in the sample are combustible and carbonaceous, the graphitic carbon referred to above. The carbonate peak in the ambient sample evolves at about 600°C; and as carbonate is not light absorbing, it does not change the optical attenuation of the sample. In addition to black carbon and carbonate, the thermograms also show several distinct groups of peaks at temperatures below $\sim$ 400°C that correspond to various organics which do not appreciably affect the optical absorption measurement.

Using this apparatus we have done a preliminary study of the relationship between the graphitic content of the aerosol and its optical absorption coefficient. A comparison of the room-temperature optical attenuation measurement with the amount of carbon represented by the high temperature peak which appears concurrently with the decrease in the sample absorptivity is shown in Fig. 12. The points in the figure include the following source emissions: highway tunnel, parking garage, oil-fired furnace, natural gas boiler, motor scooter, jet engine, and an acetylene torch. The optical attenuation and the graphitic content show a good correlation with the least squares fit corresponding to a specific attenuation of 20. Further studies are under way to test the generality of these results.

IV. Soot in the Arctic

Recent studies in the Arctic [15,16] show the presence of large aerosol concentrations which significantly affect optical transfer through the atmosphere and lead to the phenomenon of Arctic haze, which was first reported by Mitchell [17]. In particular, the observation of substantial concentrations of particulate sulfur and vanadium at the NOAA-GMCC sampling station near Barrow, Alaska, has attracted considerable attention [15,16]. Questions have been raised as to the anthropogenic character, sources, and climatic impacts of

these aerosols. In order to gain a better understanding of these issues, a study of the physical and chemical properties of the carbonaceous aerosol at Barrow was initiated in October 1979.

Recent studies of the urban aerosol indicate the presence of substantial graphitic carbon concentrations. These graphitic species — identified by a variety of modern analytical techniques (Raman spectroscopy [1], photoacoustic spectroscopy [2], thermal analysis [4], etc.) — are very effective absorbers of visible radiation and are responsible for the high optical absorption coefficients which have recently been observed in urban air [3,7]. The impacts of these highly absorbing particles on a regional or global scale have not been assessed so far, but they could be important, especially over regions with a high surface albedo like the polar icecaps. Furthermore, graphitic carbon can only be produced from combustion processes, and therefore it can offer a very attractive and convenient tracer for anthropogenic activity.

An aerosol sampler was constructed to collect parallel 47-mm quartz fiber and Millipore filter samples at a flow rate of $\sim$ 1.5 cfm. The sampler had two chambers — a lower chamber which contained the pumps and an upper chamber for collecting the aerosol samples. The upper chamber was warmed by several thermostatically controlled heatlamps, while temperature control in the lower chamber was achieved by using a thermostatically controlled fan and heatlamps. The exhaust of the pumps was vented below the sampling platform. To minimize local contamination, the aerosol sampler was controlled by a wind sensor which was built by the University of Rhode Island group [15]. This allowed samples to be collected only when the wind was from the clean air sector at Barrow, between 0° North and 130° Southeast. Results obtained with and without the wind controller suggest that there is no significant influence from local sources. Approximately 50 filter pairs have been collected at sampling time

intervals ranging from 2 days to 1 week. The quartz filters were used to determine the total carbon content of the aerosol by a combustion method [18], and the Millipore substrate was used to determine the optical absorption coefficient of the aerosol by the LBL laser transmission method. The absorption coefficients reported here are consistent with the optical constants of graphitic carbon and are expected to have an accuracy of better than a factor of 2. The Millipore substrate was also analyzed by the X-ray fluorescence technique to determine the concentration of elements with $Z > 11$. The quartz blanks had a carbon loading of $< .5\ \mu g/cm^2$, while typical filter deposits corresponded to $15\ \mu g/cm^2$. Selected filters have been analyzed by Raman spectroscopy, thermal analysis, and solvent extraction techniques. The results of these analyses are described below.

Raman spectroscopy is a highly selective method of analysis which has been used to identify large concentrations of graphitic carbon in urban particulates [1]. This technique has been applied to the analysis of several samples collected at Barrow. The results are shown in Fig. 6, where the spectrum of an Arctic sample collected in December 1979 is compared to that of urban particulates, various source emissions, and carbon black. All these spectra show the presence of two intense Raman modes located at 1350 and 1600 cm^{-1}, which have been identified as being due to phonons propagating with graphitic planes [12]. This result shows that graphitic structures similar to carbon black and due to combustion processes are present in the Arctic aerosol. Furthermore, the large intensity in these modes indicates that, just as in urban samples, the graphitic structures represent a major component of the aerosol.

The filters collected at Barrow from fall through late spring have a grey or black appearance similar to that found for urban particulates. For the urban samples, this optically absorbing component has been identified as

graphitic carbon [1]. Preliminary measurements on a limited number of samples show that the optically absorbing species in the Arctic has a $1/\lambda$ wavelength dependence, is insoluble in a wide range of solvents, and has a high temperature stability with an oxidation threshold of approximately 500°C. These results are consistent with the properties of graphitic carbon and strongly suggest that indeed the optically absorbing species at Barrow is graphitic in nature.

The seasonal variation of the optical absorptivity (or graphitic carbon concentration) of the Barrow aerosol is shown in Fig. 13. The absorption coefficient changes by more than an order of magnitude from mid-October to early January and remains at a relatively high level throughout most of February, March, and April. It decreases substantially in May. The magnitude of the absorption coefficient during the winter and spring is comparable to that found in urban environments (Table I) (i.e., the peak values in February are only about a factor of 10 less than the average absorption coefficients in New York City and a factor of 3 less than those found in Berkeley, California, and Denver, Colorado). This absorption coefficient is large enough to produce significant optical effects. For example, an absorption coefficient of 5×10^{-6} m^{-1} extended over a pathlength of 10 km would produce an optical thickness of .05. This would be a large perturbation on the transfer of optical radiation through the atmosphere when the sun's irradiance is at a high level, as it is during part of these pollution episodes. In order to assess the importance of these effects, more detailed measurements of the seasonal variation in the optical properties (visible and infrared) and the vertical and horizontal extent of the aerosols need to be determined.

The pollution episodes observed at Barrow are not a local phenomenon but appear to be areawide with similar seasonal variations occurring at widely spaced sites across the Arctic [19,20]. This is illustrated in Fig. 14, where

a comparison of the monthly variations in the blackness of the filter deposits collected at Barrow and Mould Bay, Canada, are shown. (The samples from Mould Bay were provided by Dr. L.A. Barrie and Dr. P. Hoff of the Canadian Atmospheric Environment Service.) These sampling stations are widely separated, yet the initial onset and duration of the episodes observed at these two sites are almost identical.

Using the optical constants of graphitic carbon determined from our urban studies [21], we can make an estimate of the graphitic carbon concentration at Barrow. These results are shown in Fig. 15, where we plot the graphitic carbon concentration as a fraction of the total carbon content of the aerosol for various periods of time during the year. The results show a strong enrichment of the graphitic fraction of the carbonaceous aerosol from early to late winter. The concentration of graphitic carbon in late February is almost 40% of the carbonaceous mass. Remarkably, this percentage is higher than that found in urban centers like New York City and Los Angeles [22]. After its peak in February, the fraction of graphitic carbon seems to level off to a value which is more typical of those found in urban environments. The interpretation of these intereating features in terms of transport, atmospheric chemistry, and deposition processes is complicated and will have to await more detailed analyses and further measurements.

In summary, these observations indicate that large graphitic concentrations can develop at remote locations. If one ignores the possible contribution of natural burning processes (e.g., forest fires), which are expected to be small during these times of the year in the northern hemisphere, this component can be attributed directly to the burning of fossil fuels. The source and the climatic effects of these highly absorbing species are uncertain and will have to await more systematic measurements and careful modelling.

References

1. H. Rosen, A.D.A. Hansen, L. Gundel, and T. Novakov, "Identification of the optically absorbing component in urban aerosols," Appl. Opt. 17, 3859 (1978).

2. Z. Yasa, N.M. Amer, H. Rosen, A.D.A. Hansen, and T. Novakov, "Photoacoustic investigation of urban aerosol particles," Appl. Opt. 18, 2528 (1979).

3. M. Sadler, R.J. Charlson, H. Rosen, and T. Novakov, "An intercomparison of the integrating plate and the laser transmission methods for determination of aerosol absorption coefficients," LBL-11176 (1980).

4. R. Dod et al., "Application of thermal analysis to the characterization of nitrogenous aerosol species," LBL-10735, Ch. 8 from LBL Energy and Environment Division Annual Report, 1979 (1980).

5. C.I. Lin, M. Baker, and R.J. Charlson, "Absorption coefficient of atmospheric aerosols: A method for measurement," Appl. Opt. 12, 1356 (1973).

6. A. Rosencwaig and A. Gersho, "

J. Appl. Phys. 47, 64 (1976).

7. R.E. Weiss, A.P. Waggoner, R.J. Charlson, D.L. Thorsell, J.S. Hall, and L.A. Riley, "Studies of the optical, physical and chemical properties of light absorbing aerosols," in Proceedings, Conference on Carbonaceous Particles in the Atmosphere, Lawrence Berkeley Laboratory Report LBL-9037, p. 257 (1979).

8. R. Weiss, R.J. Charlson, A.P. Waggoner, M.B. Baker, D. Covert, D. Thorsell, and S. Yuen, "Application of directly measured aerosol radiative properties to climate models," in Atmospheric Aerosols: Their Optical Properties and Effects, NASA Report CP-2004.

9. H. Rosen and T. Novakov, "Raman scattering and the characterization of atmospheric aerosol particles," Nature 266, 708 (1977).

10. H. Rosen and T. Novakov, "Identification of primary particulate carbon

and sulfate species by Raman spectroscopy," Atmos. Environ. 12, 923 (1978).

11. J.J. Blaha, G.J. Rosasco, and E.S. Etz, "The analysis of discrete fine particles by Raman spectroscopy, Appl. Spectros. 29, 396 ( ).

12. F. Tuinstra and J.L. Koenig, "Raman spectrum of graphite," J. Chem. Phys. 53, 1126 (1970).

13. H. Rosen, A.D.A. Hansen, L. Gundel, and T. Novakov, "Identification of the graphitic carbon component of source and ambient particulates by Raman spectroscopy and an optical attenuation technique," in Proceedings, Conference on Carbonaceous Particles in the Atmosphere, Lawrence Berkeley Laboratory Report LBL-9037, p. 49 (1979).

14. H. Malissa, H. Puxbaum, and E. Pell, "Zur simultanen relativkondukto-metrischen Kohlenstoff- und Schwefelbestimmung in Stäuben," Z. anal. Chem. 282, 109 (1976).

15. K.A. Rahn and R.J. McCaffrey, "On the origin and transport of the winter Arctic aerosol," in Proceedings, Conference on Aerosols: Anthropogenic and Natural - Sources and Transport, New York, Academy of Sciences, 9-12 January 1979 (in press).

16. G.E. Shaw and K. Stamnes, "Artic haze: Perturbation of the polar radiation budget," in Proceedings, Conference on Aerosols: Anthropogenic and Natural - Sources and Transport, New York, Academy of Sciences, 9-12 January 1979 (in press).

17. M. Mitchell, "Visual range in the polar regions with particular reference to the Alaskan Arctic," J. Atmos. Terr. Phys., Spec. Suppl, 195 (1956).

18. P.K. Mueller, R.W. Mosley, and L.B. Pierce, "Carbonate and non-carbonate carbon in atmospheric particulates," Second International Clean Air Congress, Proceedings (New York, Academic, 1971).

19. L.A. Barrie et al., paper presented at Second Symposium on Arctic Air Chemistry, Kingston, Rhode Island, 6-8 May 1980.

20. B. Ottar et al., paper presented at Second Symposium on Arctic Air Chemistry, Kingston, Rhode Island, 6-8 May 1980.

21. A.D.A. Hansen et al., "The use of an optical attenuation technique to estimate the carbonaceous component of urban aerosols," LBL-10735, Chap. 8 from LBL Energy and Environment Division Annual Report, 1979 (1980).

22. H. Rosen, A.D.A. Hansen, R.L. Dod, and T. Novakov, "Soot in urban atmospheres: Determination by an optical absorption technique," Science 208, 741 (1980).

Table I.

Site	Date	Number of samples	Average absorption coefficient x 10^5 (m^{-1})	Average total carbon ($\mu g/m^3$)	Average graphitic carbon as percent of total carbon[a]
Barrow, Alaska	12/79-4/80	33	.4	1.2	24
Argonne, Illinois	1/79-3/80	438	2.8	8.1	22
Gaithersburg, Maryland	1/79-3/80	381	2.1	6.1	22
Denver, Colorado	11/78-5/79	141	2.4	9.8	16
Anaheim, California	8/77-1/80	852	4.9	16.6	19
Fremont, California	7/77-3/80	924	3.4	12.0	18
Berkeley, California	6/77-4/80	998	2.1	6.7	20
New York, New York	11/78-4/80	439	6.4	15.2	27

[a]Calculated from optical constants in Ref. 13.

Figure Captions

Figure 1. Schematic of LBL laser transmission apparatus (XBL 787-1361).

Figure 2. Photoacoustic experimental arrangement (XBL 794-1230).

Figure 3. Plot of S_{ph} vs. S_{op} for various samples:

▽ - Fremont; □ - Anaheim; ○ - Denver; △ - New York City;

▪ - highway tunnel; ● - acetylene torch.

The solid line is a least squares fit of the data (XBL 794-1229).

Figure 4. Schematic of experimental arrangement used for model calculation (XBL 791-280).

Figure 5. Light absorption coefficient, $\sigma_{ab}(m^{-1})$, determined by the integrating plate method on Nuclepore filters versus $\sigma_{ab}(m^{-1})$ determined on Millipore (X) and quartz (O) filters (XBL 8010-12375).

Figure 6. Raman spectrum of an Arctic sample compared to those of urban particulates, various source emissions, carbon black, and polycrystalline graphite (XBL 767-3091A).

Figure 7. Plot of integrated Raman intensity of the 1600 cm^{-1} mode versus percent optical attenuation at 633 nm for ambient, acetylene soot, and tunnel samples (XBL 782-177).

Figure 8. Optical-thermal analysis apparatus (XBL 791-167).

Figure 9. Example of combustion thermograms of particulate material emitted from stationary sources. Dashed line is optical transmission (XBL 791-156A).

Figure 10. Example of combustion thermograms of particulate material emitted from mobile sources. Dashed line is optical transmission (XBL 791-155A).

Figure 11. CO_2 thermogram of Berkeley ambient aerosol particles (5/31/79) (XBL 807-1696).

Figure 12. Graph of optical attenuation versus carbon represented by high-temperature thermogram peak. Line is best fit to points (XBL 807-3462).

Figure 13. Seasonal variations in the optical absorption coefficient in m^{-1} at Barrow from October 1979 to May 1980 (XBL 8010-4418).

Figure 14. A comparison between the seasonal variation in the blackness of filter deposits collected at Barrow, Alaska, and Mould Bay, Canada, in 1979 and 1980. Mould Bay samples were provided by L.A. Barrie and P. Hoff of the Canadian Atmospheric Environment Service (XBL 8010-4420).

Figure 15. Seasonal variation of graphitic carbon as a percentage of the total carbon content of the aerosol at Barrow from October 1979 to May 1980. These values are compared to the average values obtained in New York City and Los Angeles (XBL 809-2013).

This manuscript was printed with figures provided by the author.

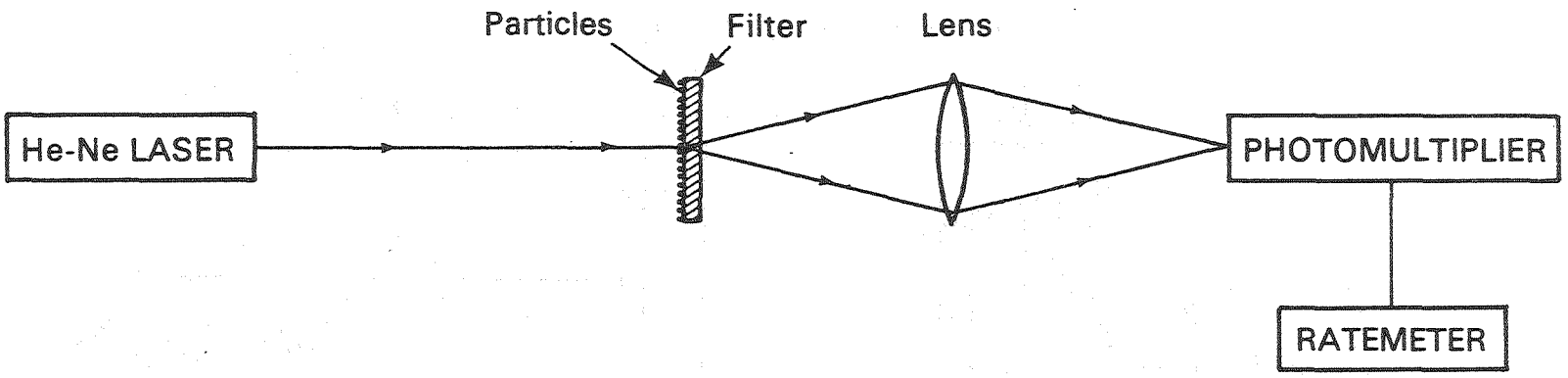

XBL 787-1361

Figure 1

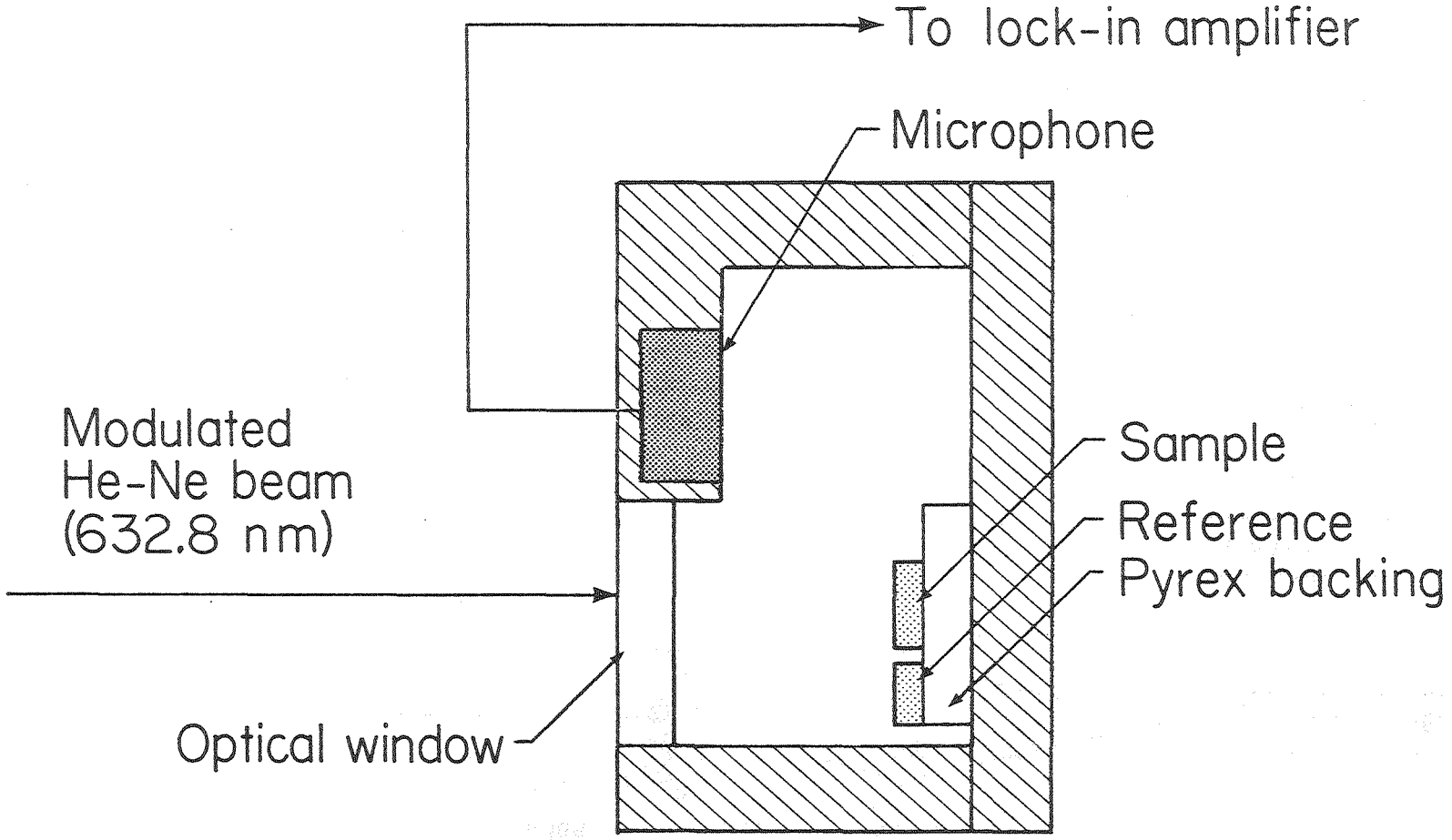

XBL 794-1230

Figure 2

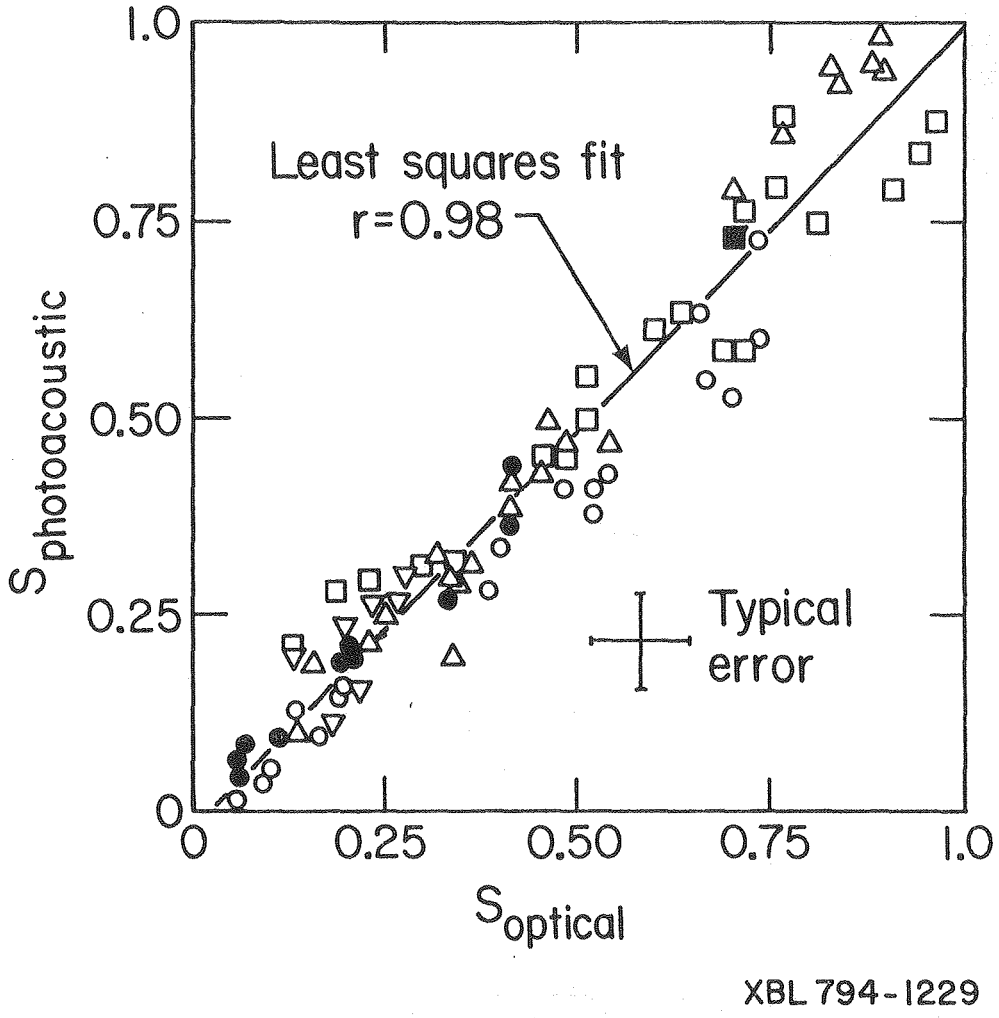
1.0
0.75
0.50
0.25
0
0
0.25
0.50
0.75
1.0
Least squares fit
r=0.98
Typical
error
S photoacoustic
S optical
XBL 794-1229

Figure 3

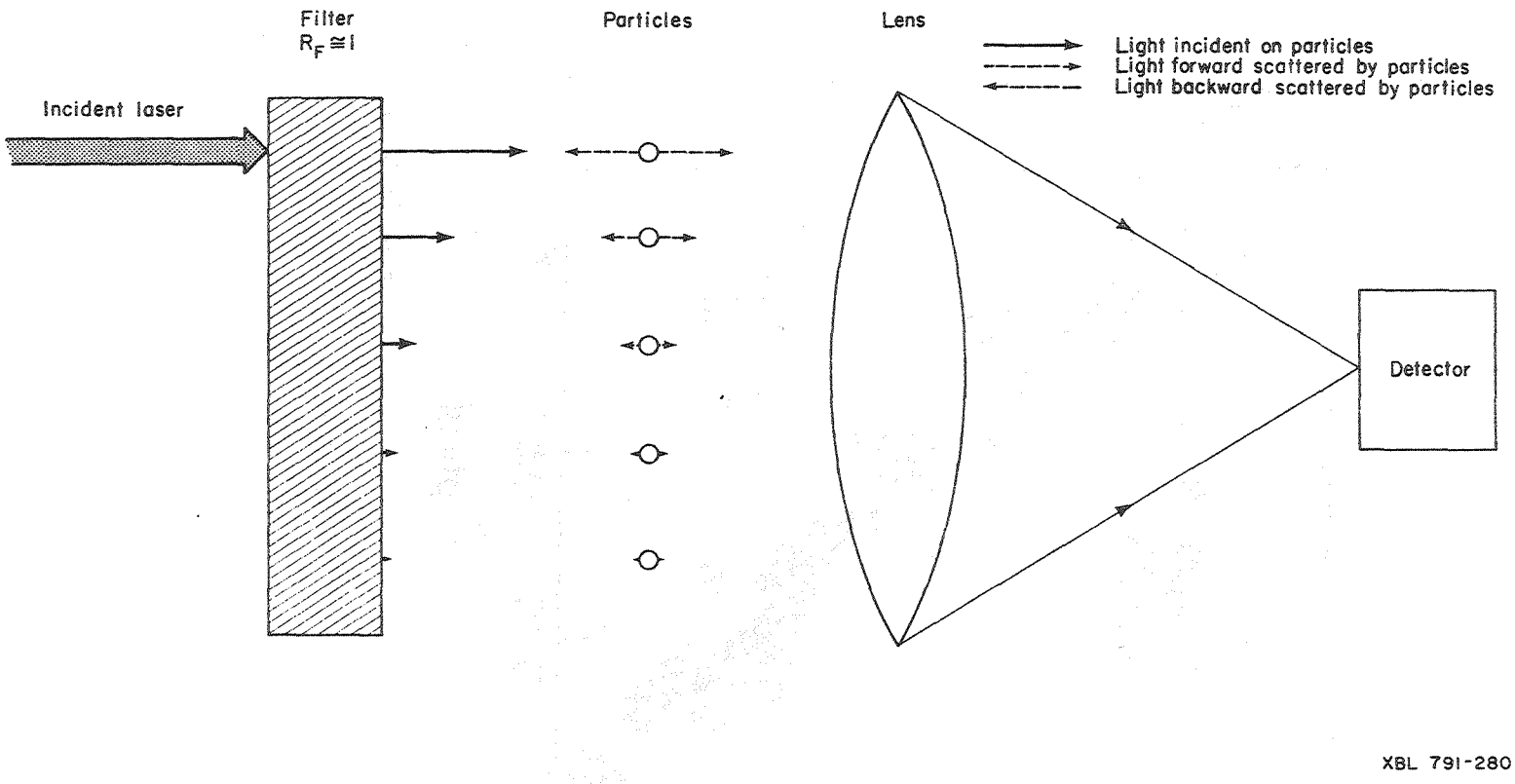
Filter
$R_F \cong 1$
Particles
Lens
Light incident on particles
Light forward scattered by particles
Light backward scattered by particles
Incident laser
Detector
XBL 791-280

Figure 4

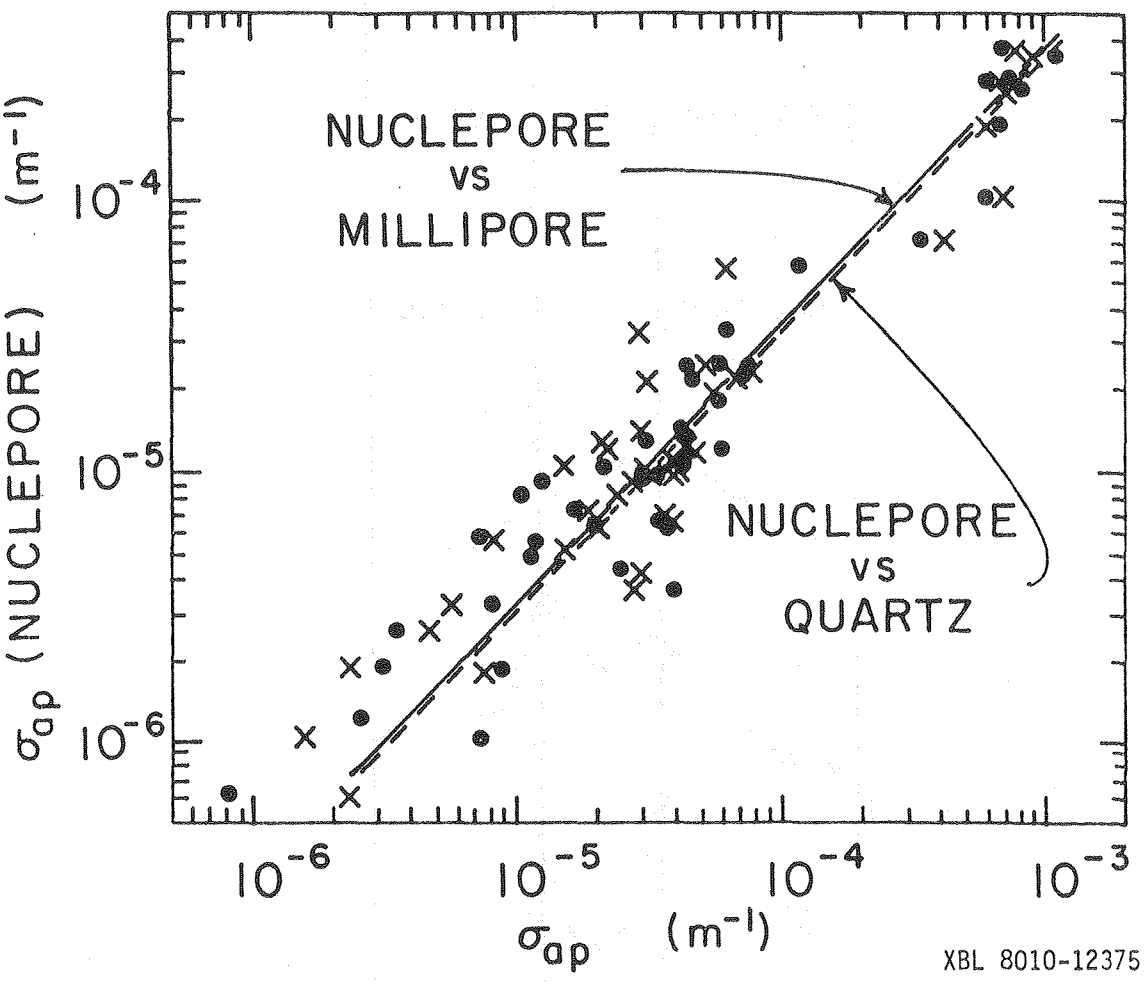
NUCLEPORE
vs
MILLIPORE
NUCLEPORE
vs
QUARTZ
σ_{ap} (NUCLEPORE) (m^{-1})
10^{-4}
10^{-5}
10^{-6}
10^{-6}
10^{-5}
10^{-4}
10^{-3}
σ_{ap} (m^{-1})
XBL 8010-12375

Figure 5

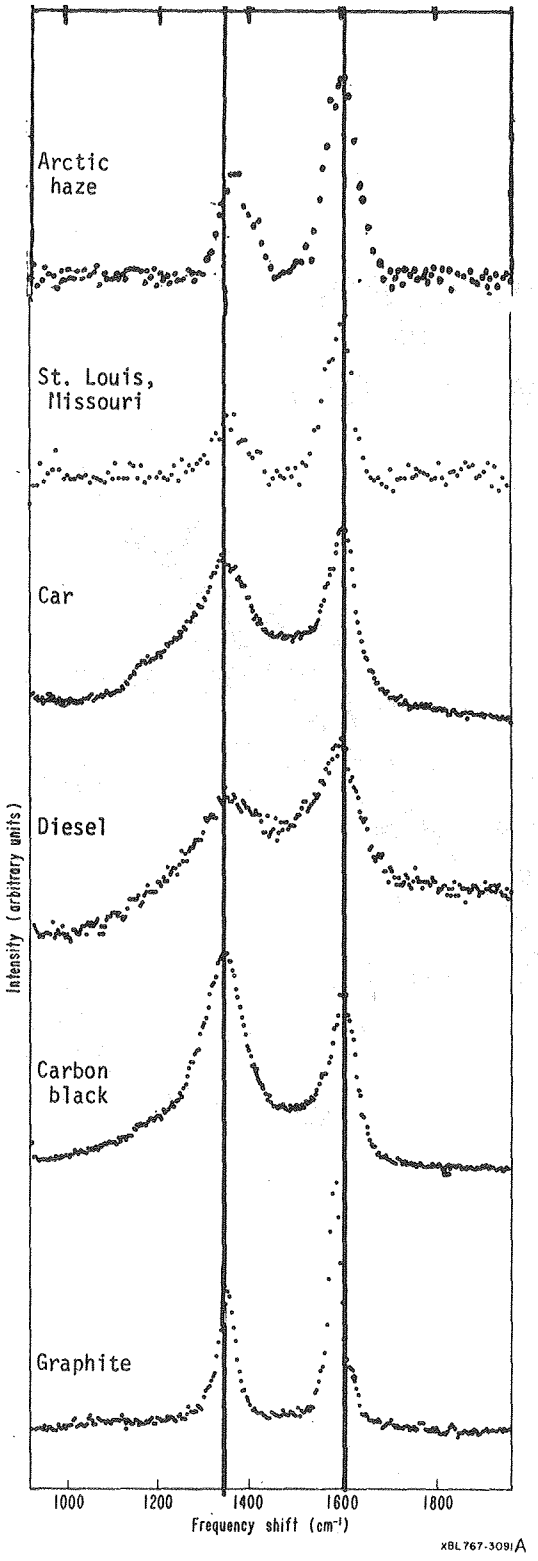
Arctic haze
St. Louis, Missouri
Car
Diesel
Carbon black
Graphite
Intensity (arbitrary units)
1000
1200
1400
1600
1800
Frequency shift (cm⁻¹)
XBL767-3091A

Figure 6

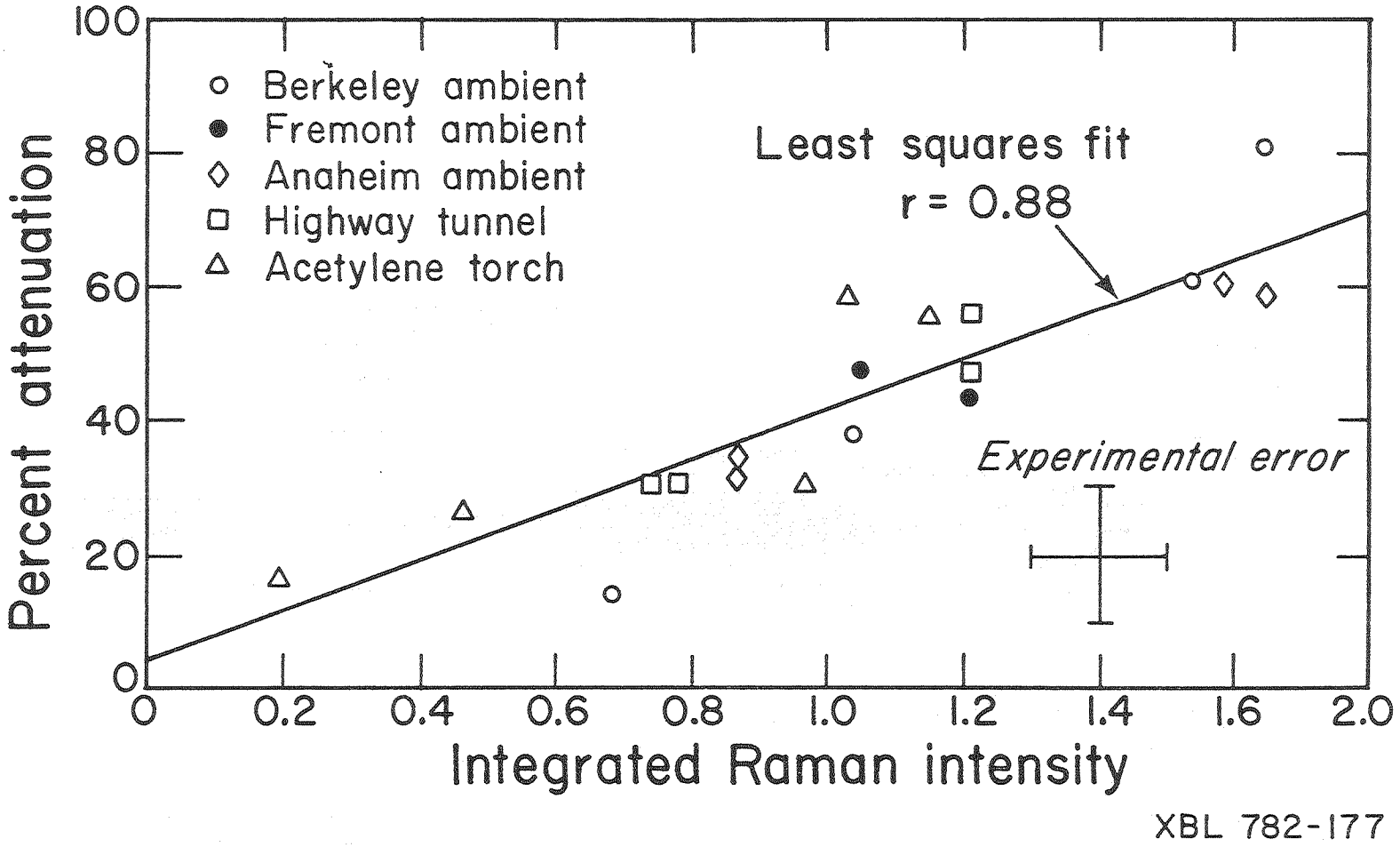
Percent attenuation
Integrated Raman intensity
Berkeley ambient
Fremont ambient
Anaheim ambient
Highway tunnel
Acetylene torch
Least squares fit
r = 0.88
Experimental error
0
20
40
60
80
100
0
0.2
0.4
0.6
0.8
1.0
1.2
1.4
1.6
2.0
XBL 782-177

Figure 7

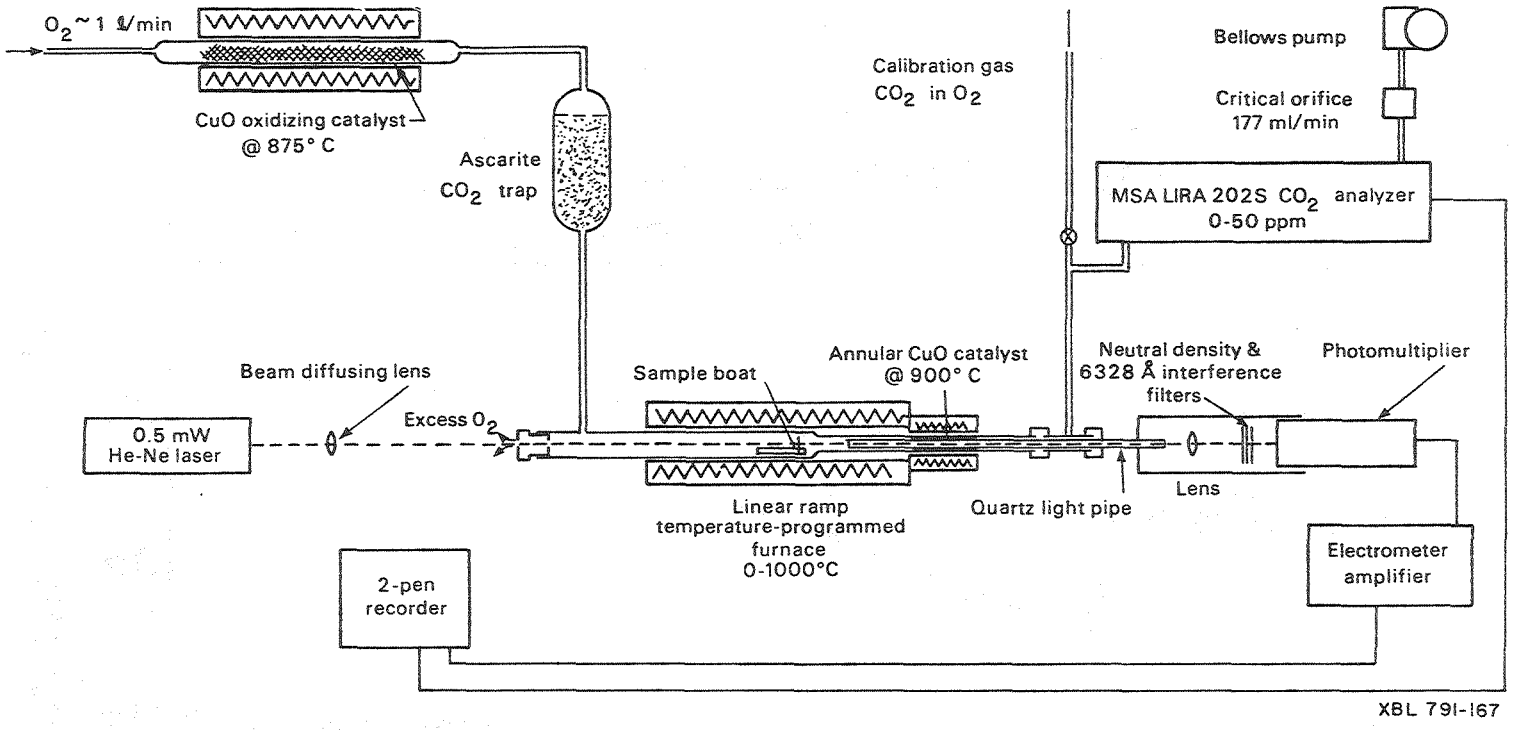
O_2 ~ 1 ℓ/min
CuO oxidizing catalyst
@ 875° C
Ascarite
CO_2 trap
Calibration gas
CO_2 in O_2
Bellows pump
Critical orifice
177 ml/min
MSA LIRA 202S CO_2 analyzer
0-50 ppm
Beam diffusing lens
Excess O_2
0.5 mW
He-Ne laser
Sample boat
Annular CuO catalyst
@ 900° C
Neutral density &
6328 Å interference
filters
Photomultiplier
Lens
Quartz light pipe
Linear ramp
temperature-programmed
furnace
0-1000°C
2-pen
recorder
Electrometer
amplifier
XBL 791-167

Figure 8

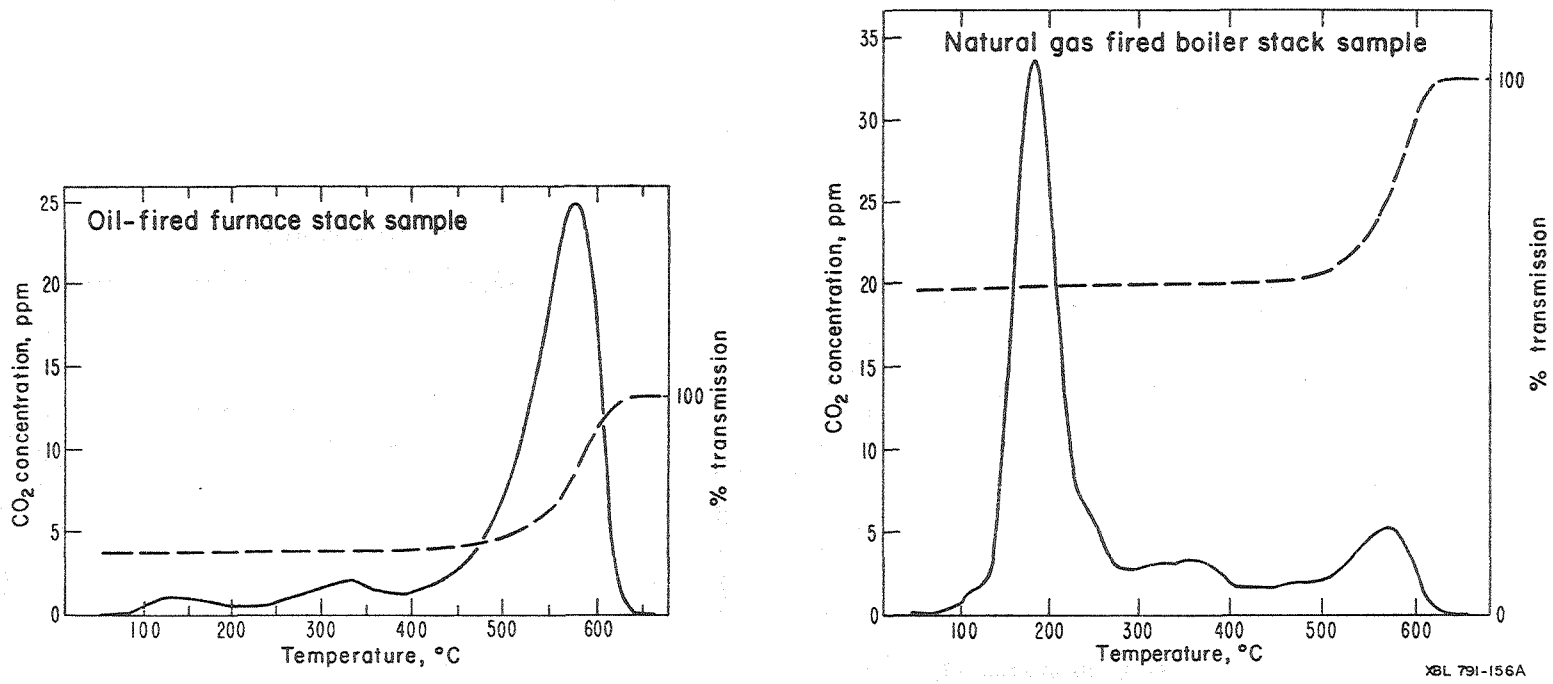
Oil-fired furnace stack sample
CO_2 concentration, ppm
% transmission
Temperature, °C
Natural gas fired boiler stack sample
CO_2 concentration, ppm
% transmission
Temperature, °C
XBL 791-156A

Figure 9

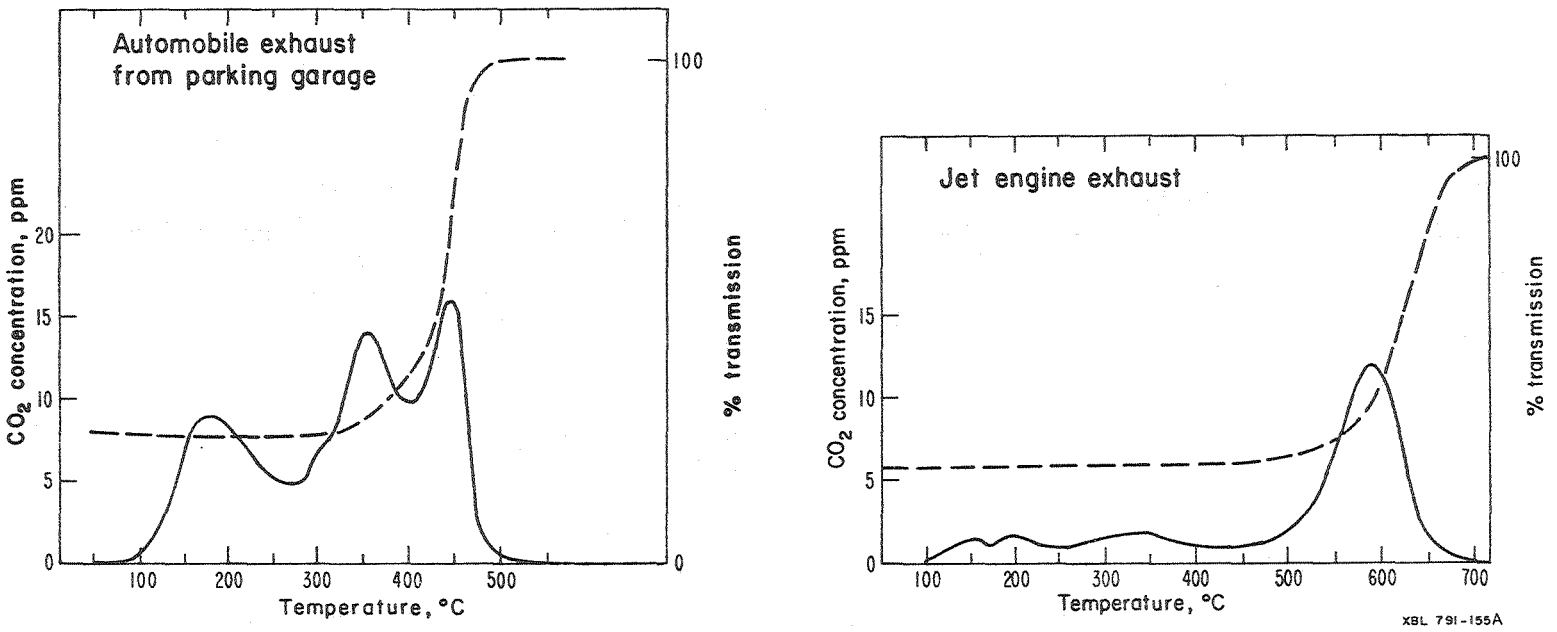
Automobile exhaust
from parking garage
CO_2 concentration, ppm
% transmission
Temperature, °C
Jet engine exhaust
CO_2 concentration, ppm
% transmission
Temperature, °C
XBL 791-155A

Figure 10

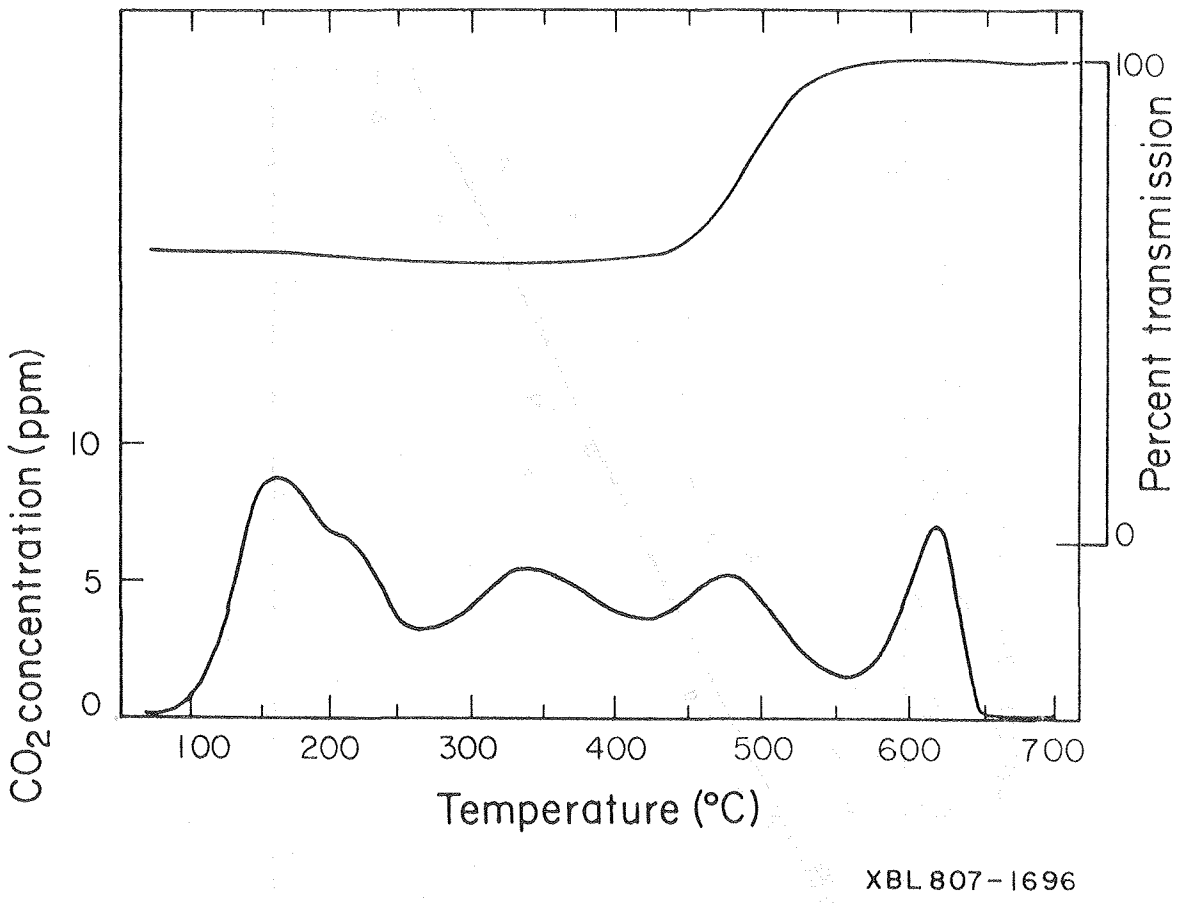
100
Percent transmission
0
10
5
0
CO_2 concentration (ppm)
100
200
300
400
500
600
700
Temperature (°C)
XBL 807-1696

Figure 11

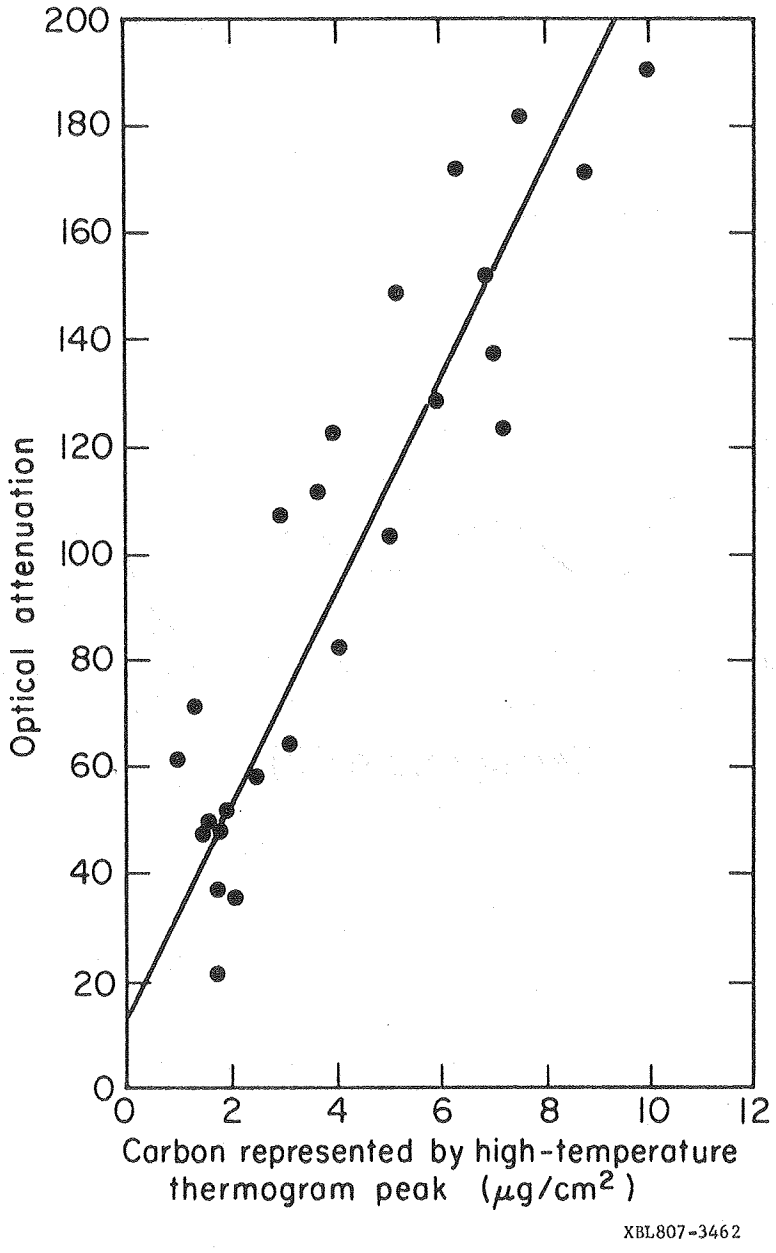
200
180
160
140
120
100
80
60
40
20
0
Optical attenuation
0
2
4
6
8
10
12
Carbon represented by high-temperature thermogram peak (μg/cm²)
XBL807-3462

Figure 12

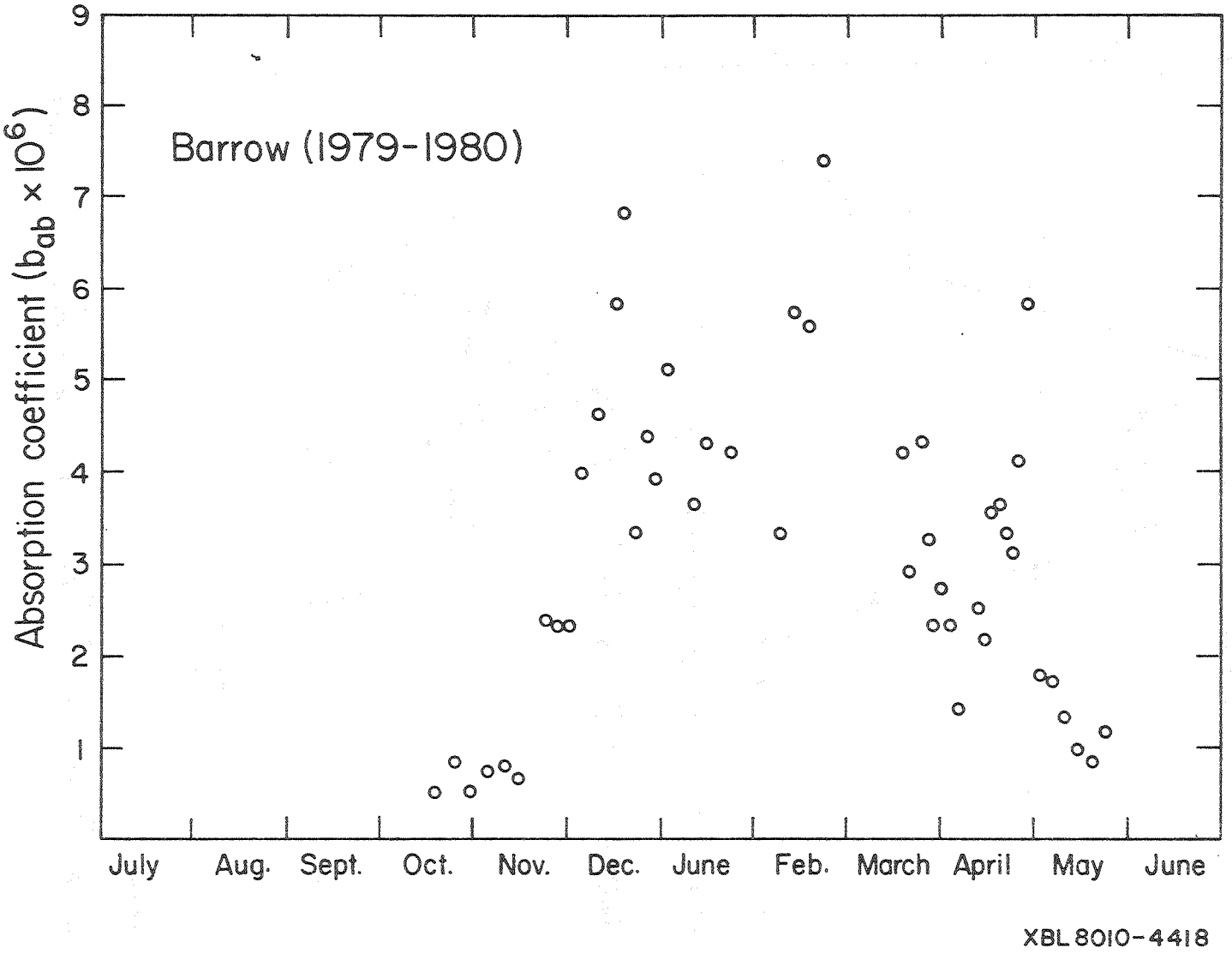
Barrow (1979-1980)
Absorption coefficient ($b_{ab} \times 10^6$)
9
8
7
6
5
4
3
2
1
July
Aug.
Sept.
Oct.
Nov.
Dec.
June
Feb.
March
April
May
June
XBL 8010-4418

Figure 13

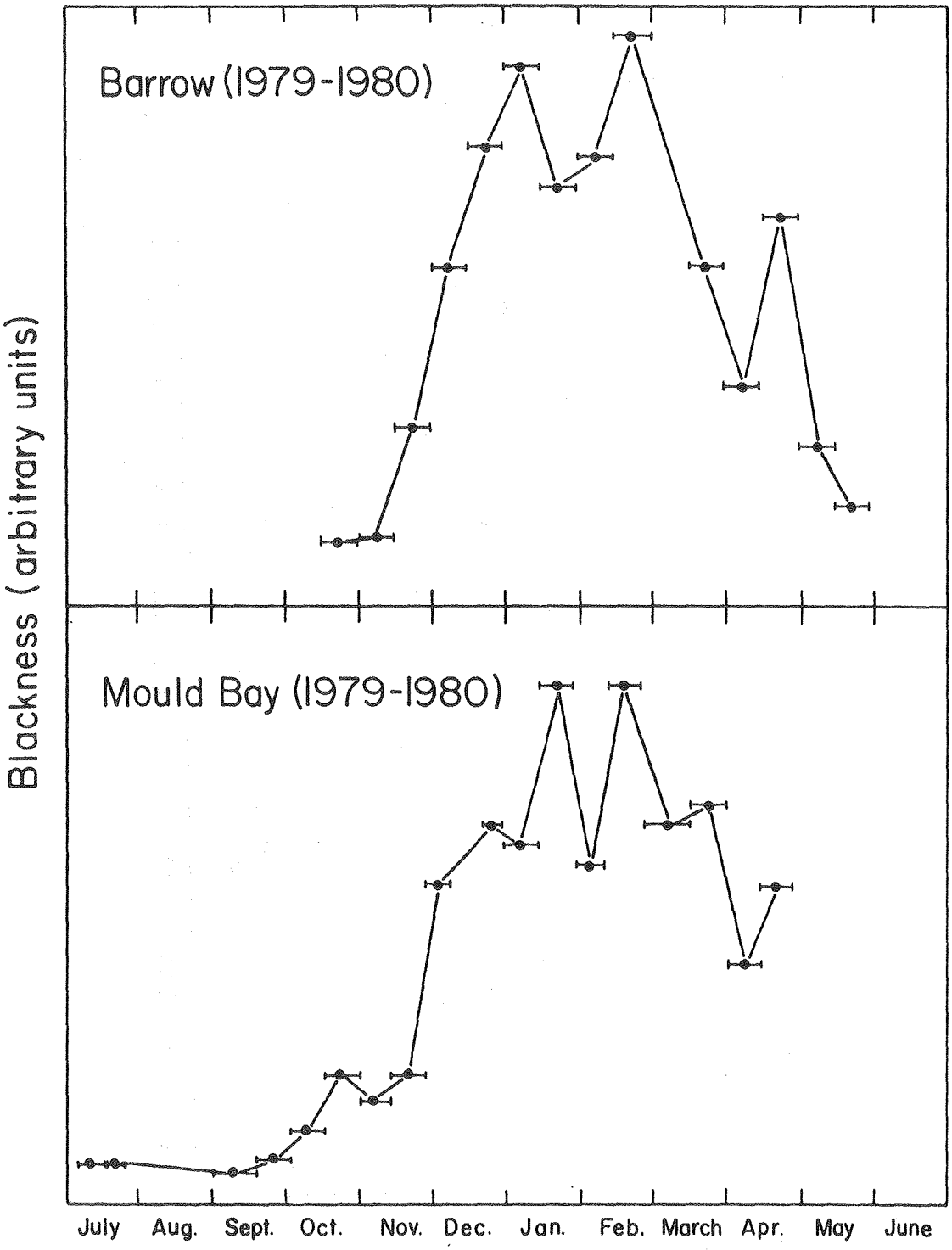
Barrow (1979-1980)
Mould Bay (1979-1980)
Blackness (arbitrary units)
July
Aug.
Sept.
Oct.
Nov.
Dec.
Jan.
Feb.
March
Apr.
May
June
XBL 8010-4420

Figure 14

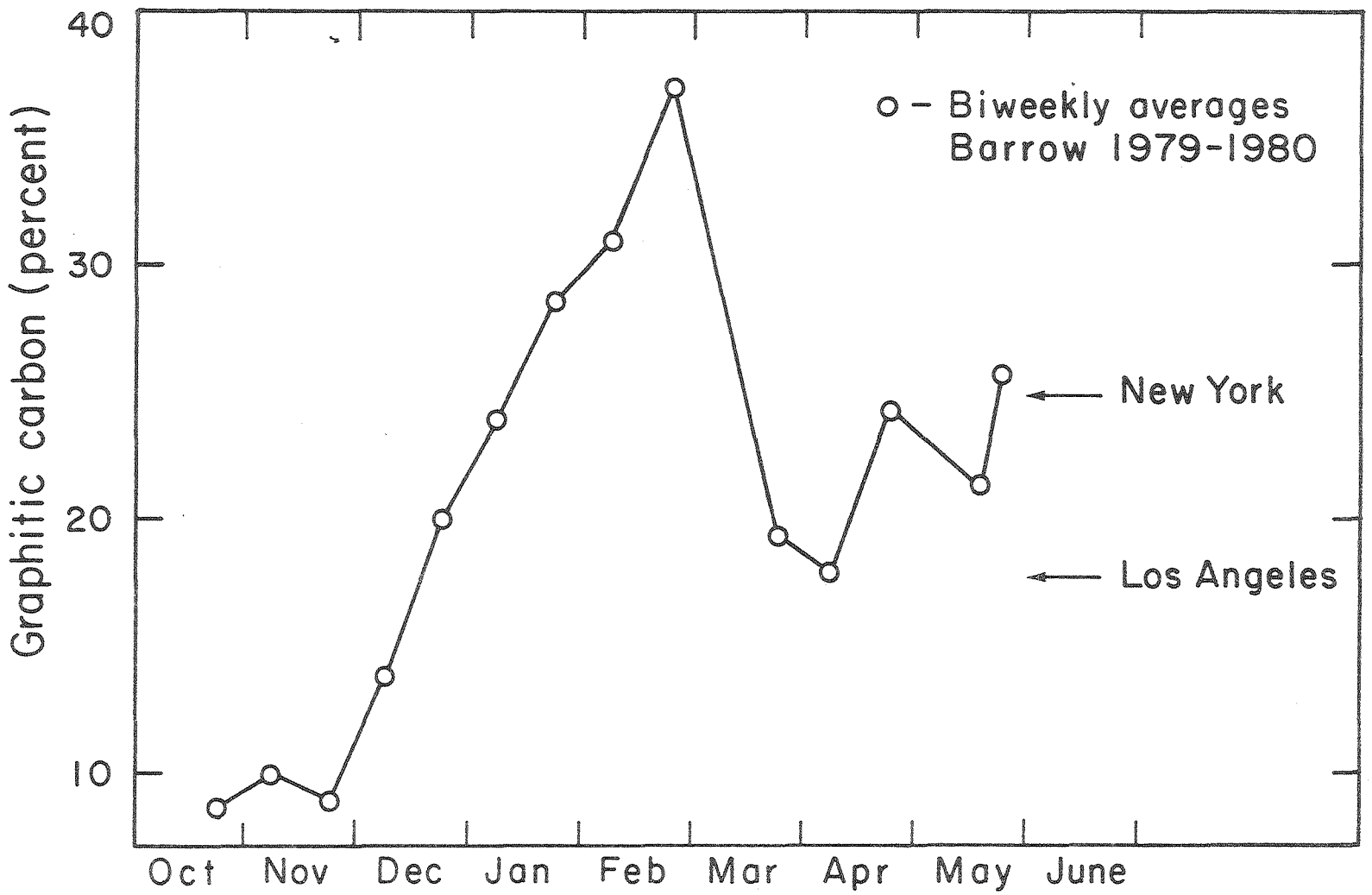

XBL 809-2013

Figure 15